Supplementary Information

Unveiling the Performance of Ultrathin Bimetallic $Co_xNi_{1-x}(OH)_2$ Nanosheets for Pseudocapacitor and Oxygen Evolution Reaction.

Pallavi Bhaktapralhad Jagdale[a], Sayali Ashok Patil[a], ArupjyotiPathak[b], MukaddarSk[b], Ranjit Thapa[b,c], Amanda Sfeir[d], Sebastien Royer[d,e], Akshaya Kumar Samal[a], Manav Saxena[a*]

[a] Centre for Nano and Material Sciences, Jain (Deemed-to-be University), Jain Global Campus, Ramanagara, Bangalore 562112, India

[b] Department of Physics, SRM University-AP, Amaravati 522240, Andhra Pradesh, India

[c] Centre for Computational and Integrative Sciences, SRM University − AP, Amaravati 522240, Andhra Pradesh, India

[d] Université de Lille, CNRS, Centrale Lille, Université Artois, UMR 8181─UCCS─12 Unité de Catalyse et Chimie du Solide, Lille 59000, France

[e] Université du Littoral Côte d'Opale – Ecole d'Ingénieur du Littoral Côte d'Opale, UCEIV, UR 4492, MREI 1, 189 A, Avenue Maurice Schumann, 59140 Dunkerque, France.

E-mail: s.manav@jainuniversity.ac.in, manavsaxena19@gmail.com

Experimental section

Preparation of RuO_2 electrode

2 mg of RuO_2 was added to 1.6 ml of DI water, 400 µl ethanol, and 20 µl Nafion and sonicated for 30 min at room temperature. 30 µl of the RuO_2 catalytic ink was drop-casted on cleaned FTO-coated glass and dried in ambient conditions.

Material Characterization

Preparation of ICP-OES samples

The$Co_xNi_{1-x}(OH)_2$ NS were directly transferred to the silicon substrate (1x1 cm area) and immediately immersed into the vial containing 15 ml of conc. HCl solution. The vial was sonicated for 10 minutes to complete the nanosheet dispersion into the HCl, and the silicon wafer was removed prior to ICP-OES analysis.

Electrochemical measurements

All the electrochemical measurements were recorded in OrigalysElectroChem SAS, France at room temperature. In a three-electrode configuration, $Co_xNi_{1-x}(OH)_2$ NS on Pt with a working area of 0.25 cm^2, Hg/HgO, and Pt wire were used as working, reference, and counter electrodes for charge storage. The basic analysis of working electrodes was carried out by cyclic voltammetry (CV), galvanostatic charge-discharge (GCD), and electrochemical impedance spectroscopy (EIS) in a 2M KOH electrolyte. In a two-electrode (symmetric) system, two Pt substrates with Co_1Ni_3-NS were used as positive and negative electrodes and separated by filter paper soaked in 2M KOH. The electrochemical impedance spectroscopy (EIS) was performed in the frequency range from 100 kHz to 0.01 Hz at 5 mV. The areal and/or volumetric capacitance (and capacity), energy density, and power density were calculated using the below formulae.[1-3]

$$C_a = \frac{I\,\Delta t}{A\,\Delta V}$$

(1)

$$C_{vol} = \frac{I\,\Delta t}{V\,\Delta V}$$

(2)

$$Q_a = \frac{I\,\Delta t}{A}$$

(3)

$$ED = \frac{C_a \Delta V^2}{2}$$

(4)

$$PD = \frac{ED\ x\ 3600}{\Delta t}$$

(5)

Where C_a and Q_a represent the areal capacitance (F cm^{-2}) and areal capacity (Ah cm^{-2}), I, Δt, A, and ΔV respectively denote the current applied (A), discharge time (s), area of working electrode (cm^2), and potential window (V). ED (Wh cm^{-2}) and PD (W cm^{-2}) correspond to energy density and power density, respectively.

To test the electrocatalytic OER performance of $Co_xNi_{1-x}(OH)_2$ NS, NS on FTO-coated glass substrate having a working area of 0.5 cm^2, Hg/HgO, and graphite rod were used as working,

reference, and counter electrodes, respectively. The electrochemical analysis was performed in 1M aqueous KOH electrolyte at room temperature. The applied potentials were calibrated with respect to the reversible hydrogen electrode (RHE) using the following formula.[4]

$$E_{RHE} = E_{Hg/HgO} + 0.059\,pH + 0.098\,V \quad (6)$$

The Tafel slope was achieved by plotting overpotential as a function of log j based on the following equation:

$$\eta = a + b\,log\,|j| \quad (7)$$

where, η, a, b, and j respectively correspond to overpotential, Tafel constant, Tafel slope, and current density.

The CV scan was performed at a scan rate of 50 mV^{-1} between 1.2 to 1.8 V (vs RHE) until getting the stable CV curve. The linear sweep voltammetry (LSV) was measured at a scan rate of 5 mVs^{-1}. EIS of the $Co_xNi_{1-x}(OH)_2$ NS and RuO_2 were recorded in the frequency range from 100 kHz to 0.01 Hz at a constant potential of 1.55 V (vs RHE). The CV measurements were taken in the non-faradaic region (-0.1 to 0.0 V vs Hg/HgO) at different scan rates of 10 to 100 mVs^{-1} (**Fig. S14**) The electrochemically active surface area was calculated using the following formula:

$$ECSA = C_{dl}/C_s \quad (8)$$

Where the slope obtained by plotting the difference between anodic current density (J_a) and cathodic current density (J_c) (i.e. Δj at -0.5 V) against the scan rate is twice the double-layer capacitance (C_{dl}) and C_s is the specific capacitance (i.e. 40 μF cm^{-2}) which previously reported value for metal oxide/hydroxides.[5]

The mass activity (A g^{-1}) was calculated by normalizing the current density by the mass loading (l), as given in the equation below.[6]

$$Mass\ activity = j/m \quad (9)$$

Where, mass loading

$$(l) = A\ x\ \rho\ x\ effective\ thickness\ = A\ x\ \rho\ x\ \frac{Q\ x\ M}{F\ x\ A\ x\ \rho} \quad (10)$$

Turnover frequency (TOF, s^{-1}) was measured to estimate the intrinsic OER activity using the equation.

$$TOF = j\ x\ A/4\ x\ F\ x\ n \quad (11)$$

Where j and A represent the current density and area of the electrode, respectively. Whereas F and n denote Faraday's constant and moles of the electrocatalyst, respectively. Q is the quantity of electric charge (A.s) which was quantified by integrating the oxidation peak area of $Co^{3+/2+}$ and $Ni^{3+/2+}$ in the LSV polarization curve as shown in **Fig. S15.** 'ρ' is the density and 'M' is the molecular weight of $Co(OH)_2$, $Ni(OH)_2$ and bimetallic $Co_xNi_{1-x}(OH)_2$ nanosheets.

The effective density of bimetallic $Co_xNi_{1-x}(OH)_2$ NS based on mass fraction was calculated using the below equation.

$$\frac{1}{\rho_{total}} = \frac{f_{Co}}{\rho_{Co}} + \frac{f_{Ni}}{\rho_{Ni}} \qquad (f_{Co} + f_{Ni} = 1) \quad (12)$$

Where ρ is the density of cobalt and nickel (g cm^{-3}) and f is the mass fraction of Co and Ni attained from ICP-OES analysis as shown in **Table 1.**

The molecular weight of bimetallic $Co_xNi_{1-x}(OH)_2$ NS was determined using a general formula:

$$M = (x \times M_{Co}) + (y + M_{Ni}) + 2 \times (M_O + M_H) \quad (13)$$

Where, M_{Co}, M_{Ni}, M_O, and M_H are a molar mass of cobalt (58.93 g mol^{-1}), nickel (58.69 g mol^{-1}), oxygen (16.0 g mol^{-1}), and hydrogen (1.0 g mol^{-1}), respectively. 'x' and 'y' respectively signifies the stoichiometric coefficients of Co and Ni.

The effective density and molecular weight merits are given in **Table S7**.

DFT calculations

We conducted a theoretical investigation of CoNi hydroxide, focusing on its charge storage properties and catalytic activity for the oxygen evolution reaction (OER), using density

functional theory (DFT)[7] as implemented in the Vienna Ab initio Simulation Package (VASP)[8, 9]. The interaction of core electrons was modelled using the projected augmented wave (PAW)[10]pseudopotential method. The exchange-correlation interactions of electrons were treated using the Perdew-Burke-Ernzerhof (PBE) functional within the generalized gradient approximation (GGA)[11]. To achieve reliable results, the Brillouin zone was sampled with a 3x3x1 K-point grid according to the Monkhorst-Pack scheme. A kinetic energy cut-off of 450 eV for the plane wave basis set was chosen after performing convergence tests. Moreover, the ionic relaxation process was governed by an energy convergence threshold of 10^{-5} eV and a force convergence criterion of 0.01 eV/Å. This approach allowed each atom to relax until the Hellmann-Feynman forces were reduced to the specified value[8]. A supercell with dimensions 2x2x1 was constructed, consisting of 80 atoms, after cleaving the CoNi-hydroxide unit cell, which contains 20 atoms, along the (003) plane. A vacuum of 18 Å in length was applied to provide interactions between repeating images. Additionally, our calculations employed the DFT-D3 method with Becke-Johnson damping for accurate dispersion corrections[12].

The adsorption-free energies of molecules and intermediates were calculated using the following approach: Under alkaline conditions, the oxygen evolution reaction (OER) proceeds through the following steps:

$$4OH^- \longrightarrow O_2 + 2H_{2O}(l) + 4e^-$$

Pathway is,

$$4OH^- + * \quad (14)$$

$$OH^* + 3OH^- + e^- \quad (15)$$

$$O^* + H_{2O}(l) + 2OH^- + 2e^- \quad (16)$$

$$OOH^* + H_{2O}(l) + OH^- + 3e^- \quad (17)$$

$$O_2 + 2H_{2O}(l) + 4e^- + * \quad (18)$$

Here, * indicates the free surface, while $H_2O(l)$ signifies liquid water. The Gibbs free energy of an intermediate is calculated using the formula G = E + ZPE − TS − neU. In this equation, E represents the DFT energy, ZPE is the zero-point energy, TS corresponds to the entropy contribution, n denotes the number of electrons exchanged, and U is the applied potential at

the electrode. For adsorbed intermediates, the effects of ZPE and TS are negligible and can be ignored. The equilibrium potential, U_0, is 0.40 V versus RHE in an alkaline medium with a pH of 14. The basic reaction steps for the oxygen evolution reaction (OER), which are used to construct the free energy diagram, are as follows:

G (14) – G (14) (19)

G (15) – G (14) (20)

G (16) – G (14) (21)

G (17) – G (14) (22)

G (18) – G (14) (23)

We utilized the following free energy relationships for ions and molecules to calculate the total free energy of the entire reaction, setting it at 4.92 eV:

$$G_{H_2O(l)} = G_{H_2O(g)} + RT\ln\left(\frac{p}{p_0}\right) \quad (24)$$

$$G_{O_{2(g)}} = 2G_{H_2O(l)} - 2G_{H_2} + 4.92 \quad (25)$$

$$G_{OH^-} = G_{H_2O(l)} - G_{H^+} \quad (26)$$

$$G_{H^+} = \frac{1}{2}G_{H_2} - k_B \mathrm{T}\ln 10 \times \mathrm{pH} \quad (27)$$

Here, R represents the gas constant, T is set to 298.15 K, p equals 0.035 bar, and p_0 is 1 bar. The Boltzmann constant, K_B, is 8.6173332×10^{-5} eV, with a pH of 14. The DFT energies, entropy contributions, and zero-point energies for the free molecules are listed in **Table S2**.

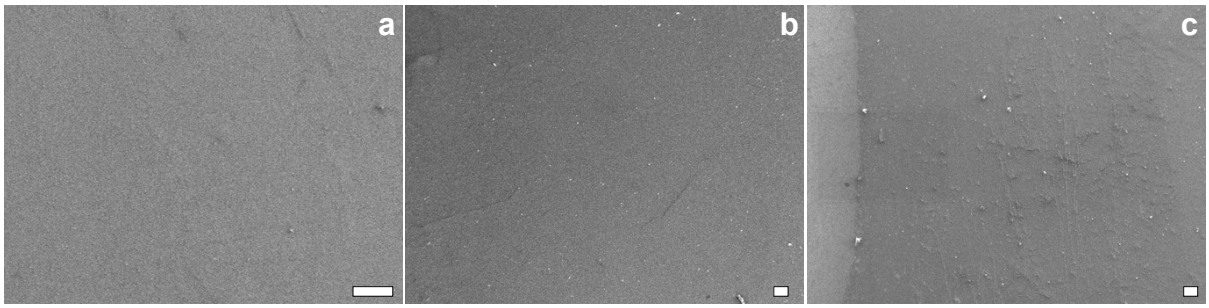

Fig. S1: FESEM images of $Co_xNi_{1-x}(OH)_2$ NSs with different ratios of Co: Ni (a) 3: 1, Co_1Ni_3-NS (b) 1: 1, Co_1Ni_1-NS (c) 1: 3, Co_3Ni_1-NS. The scale bar is 100 μm.

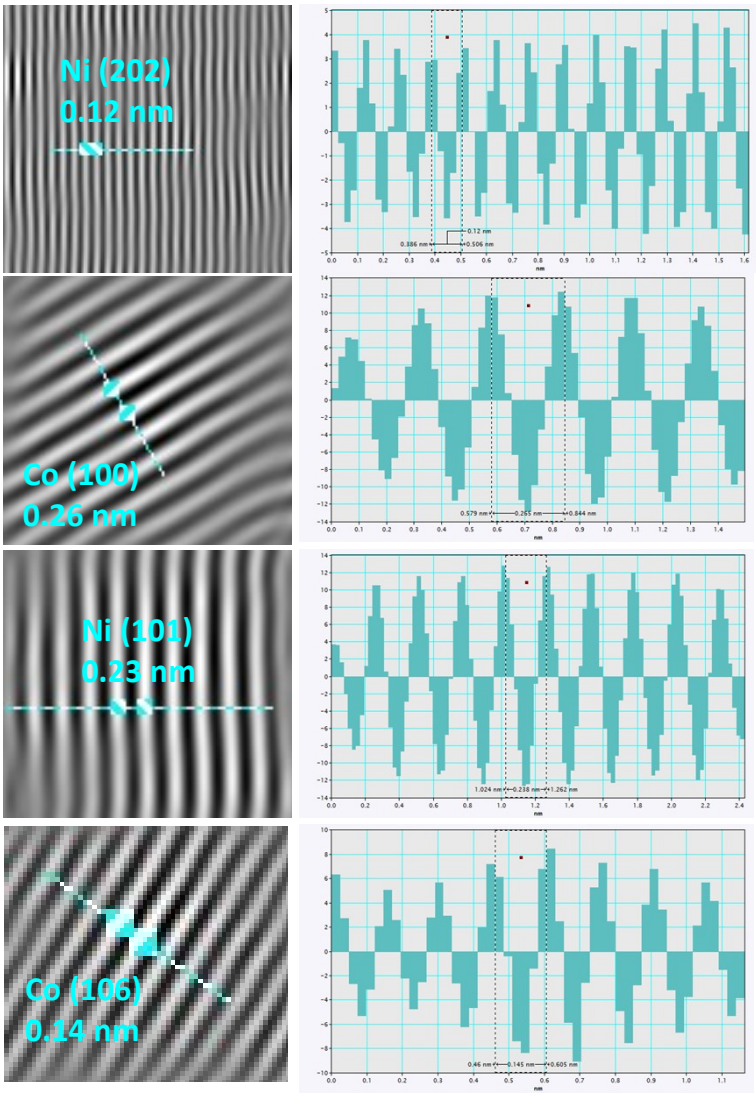

Fig. S2: IFFT and line intensity profile of HRTEM image of $Co_1Ni_3(OH)_2$ NSs (Fig. 1e) generated through Gatan software. The inter-planar spacings were analyzed using the bright spot approach.

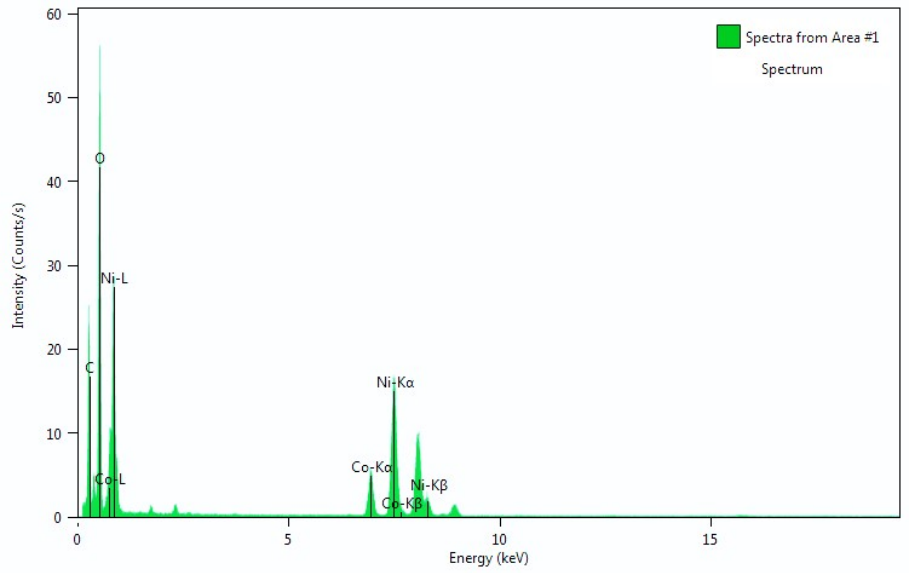

Fig. S3: EDS spectrum of Co_1Ni_3-NS showing the high ratio of Ni compared to Co inthe bimetallic-hydroxide nanosheet.

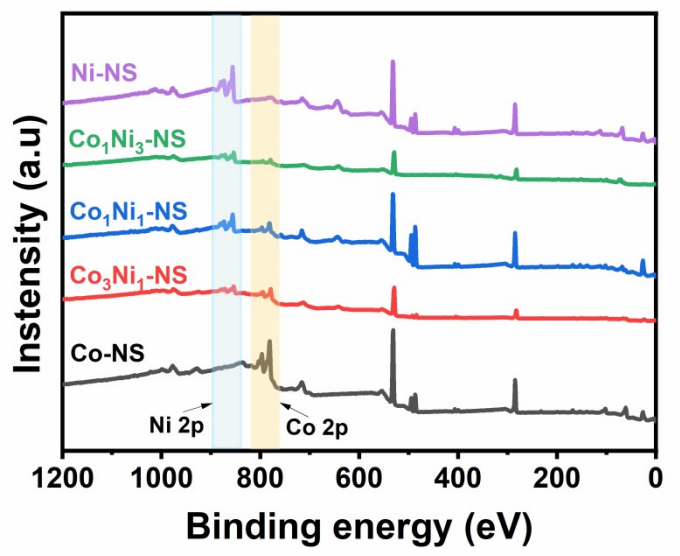

Fig. S4: Survey spectrum of $Co_xNi_{1-x}(OH)_2$ nanosheets showing elemental composition of Co and Ni.

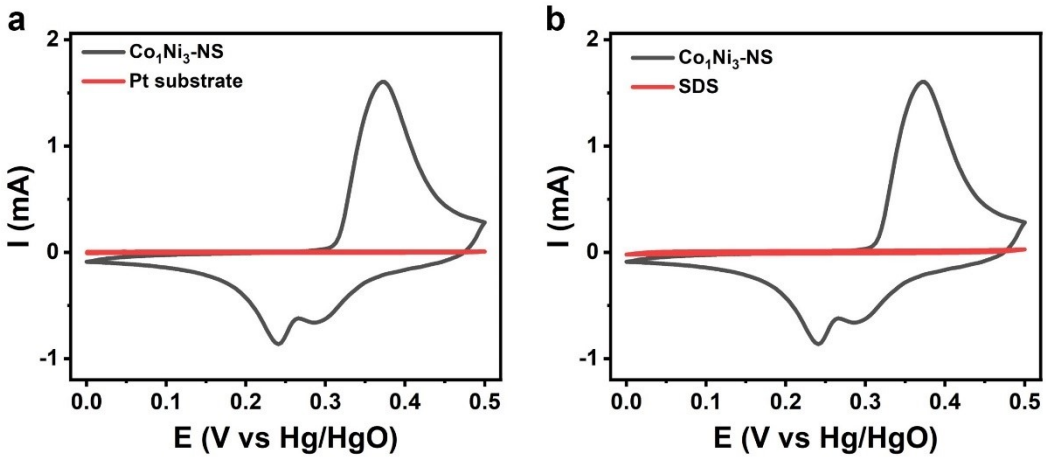

Fig. S5: The CV plot of (a) Co_1Ni_3-NS and Pt substrate,(b) Co_1Ni_3-NS and SDS on Pt substrate at 100 mV s^{-1} showing negligible capacitance contribution of Pt substrate and SDS.

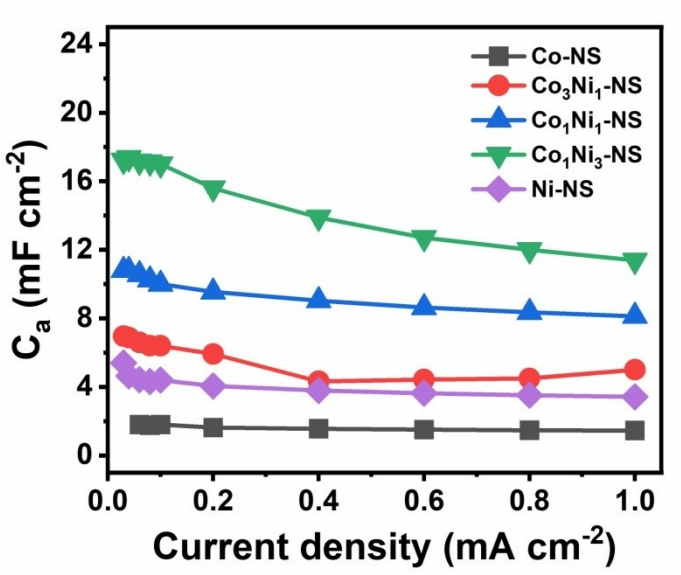

Fig. S6: Comparison of the areal capacitance of $Co_xNi_{1-x}(OH)_2$ NS electrodes at different current densities.

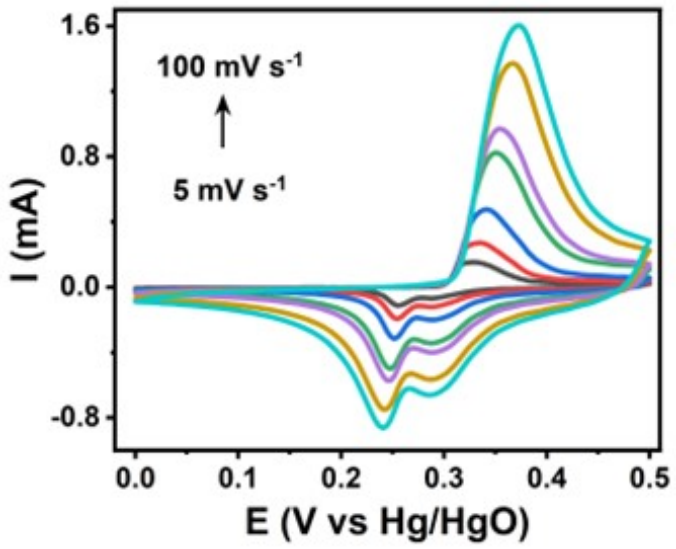

Fig. S7: CV curves of Co_1Ni_3-NS at various scan rates (5- 100 mV s^{-1}).

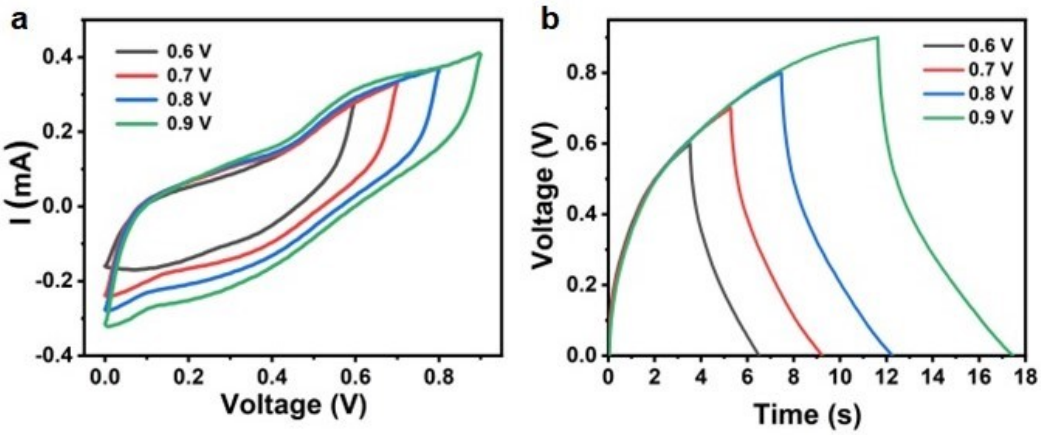

Fig. S8: (a) CV of the symmetric device based on Co_1Ni_3-NS at various potential windows at scan rate 100 mV s^{-1}, and (b) GCD at a constant current density of 0.8 mA cm^{-2}.

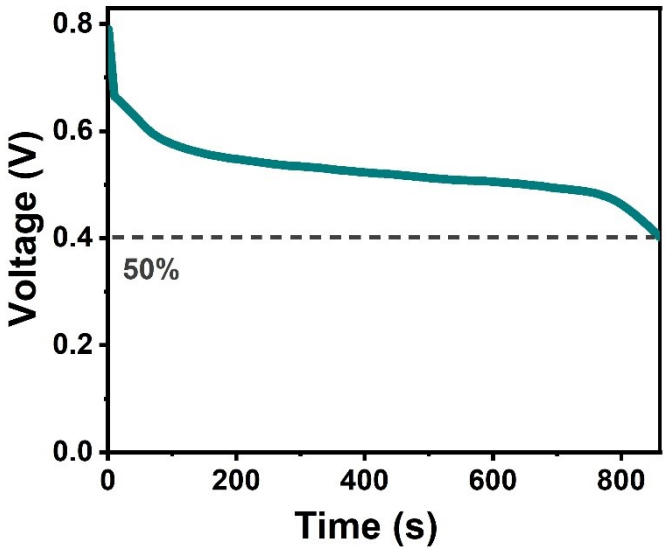

Fig. S9: Self-discharge measurements of supercapacitor device by open-circuit potential.

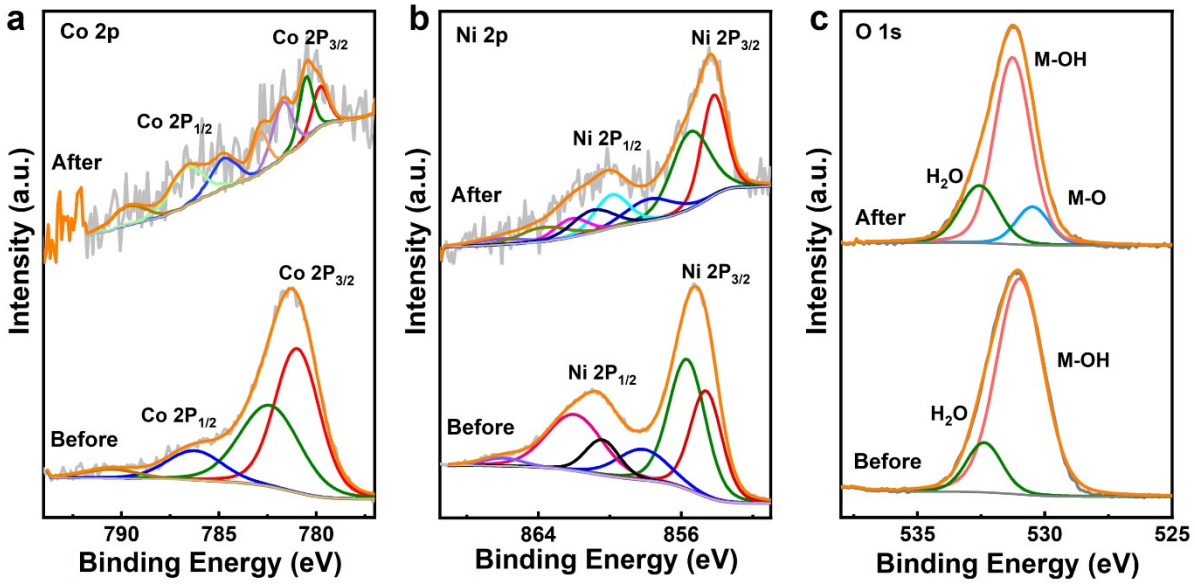

Fig. S10: XPS analysis of Co_1Ni_3-NS electrode before and after long-term cyclic stability of pseudocapacitor. (a) high resolution Co 2p spectrum,(b) Ni 2p spectrum, (c) O 1s spectrum.

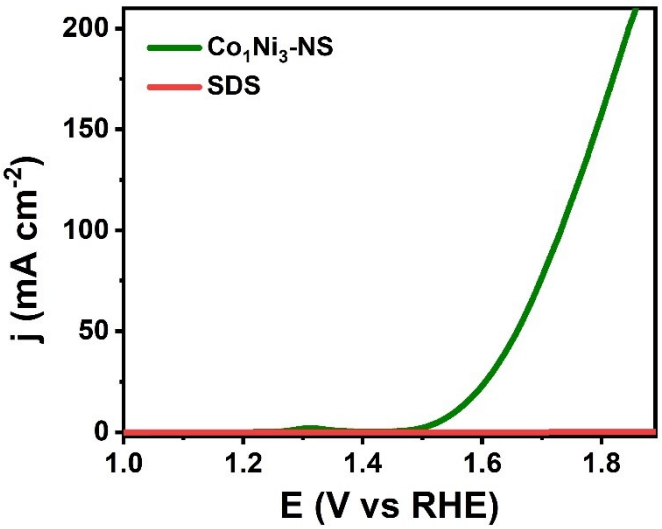

Fig. S11: LSV at 5 mVs^{-1}comparing OER performance of Co_1Ni_3-NS and SDS on FTO-coated glass substrate.

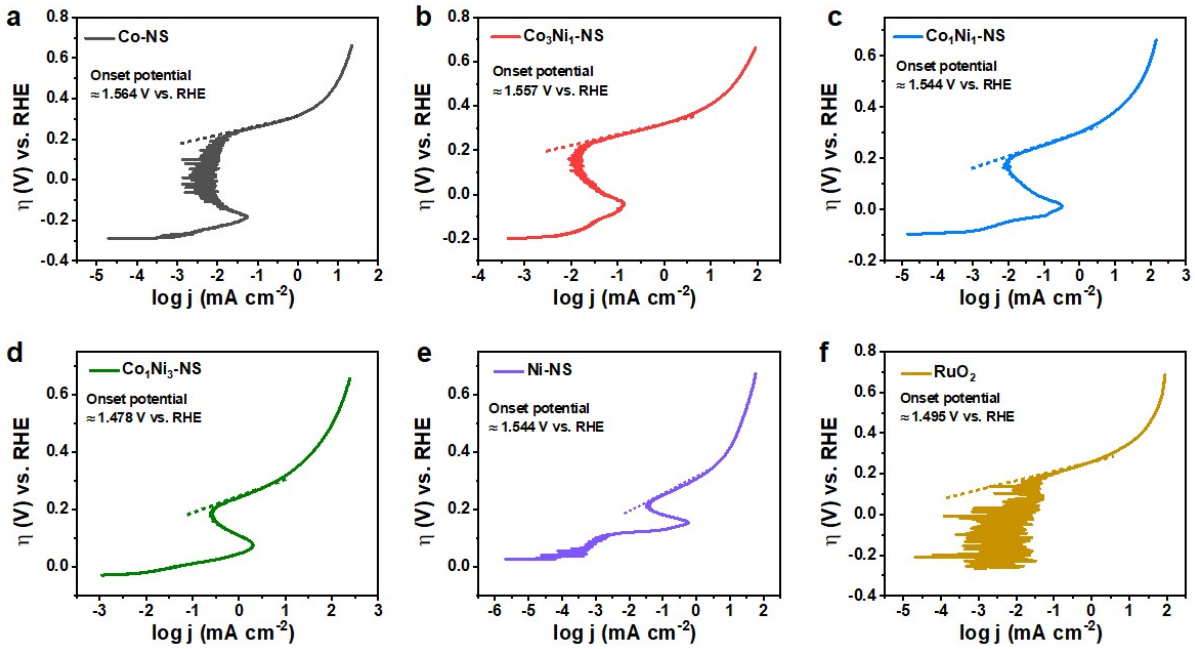

Fig. S12: Plots of overpotential versus the log (j) to determine the onset potential of (a) Co-NS, (b) Co_3Ni_1-NS, (c) Co_1Ni_1-NS, (d) Co_1Ni_3-NS, (e) Ni-NS, and (f) RuO_2.

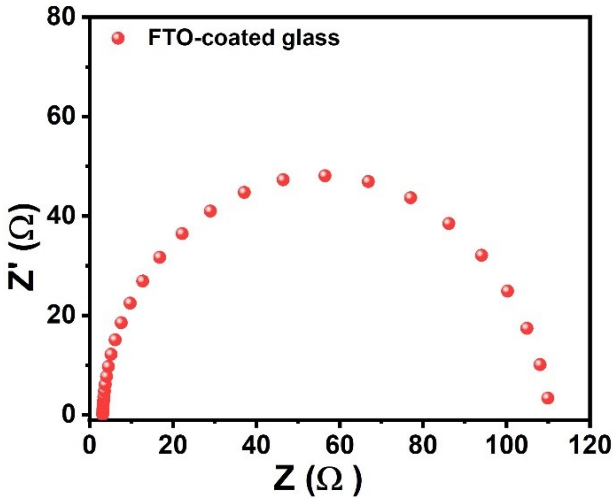

Fig. S13: Nyquist plot of FTO-coated glass substrate showing high resistance of 107 Ω.

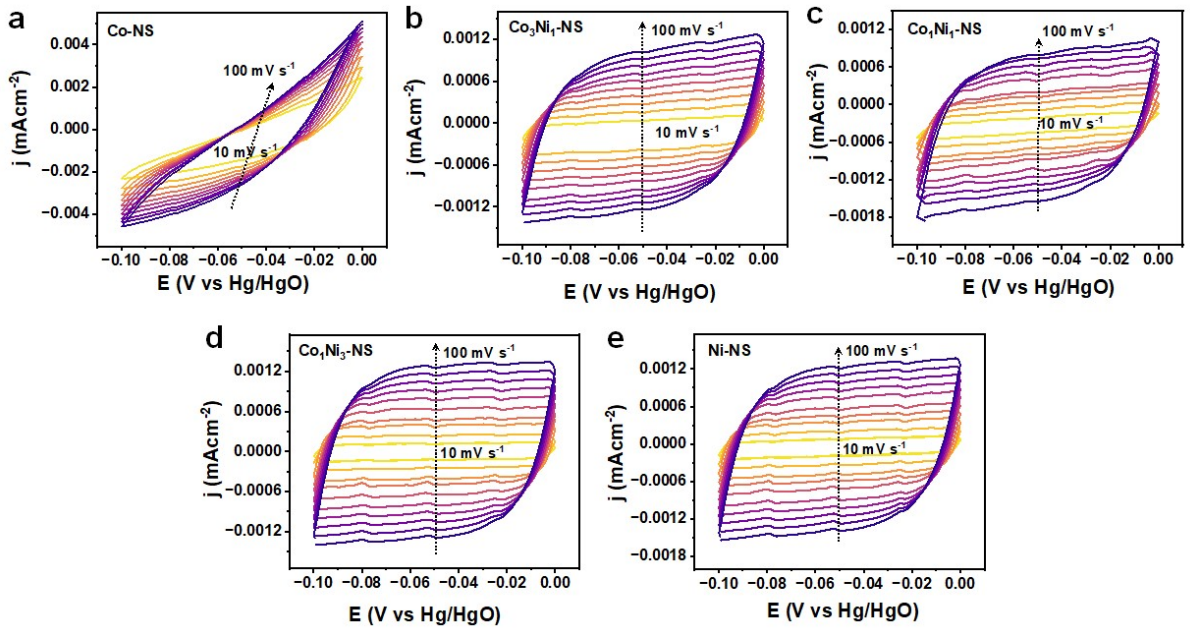

Fig. S14: CV curves recorded at a non-Faradaic region at various scan rates for bimetallic $Co_xNi_{1-x}(OH)_2$ NS electrodes (a) Co-NS, (b) Co_3Ni_1-NS, (c) Co_1Ni_1-NS, (d) Co_1Ni_3-NS, and (e) Ni-NS.

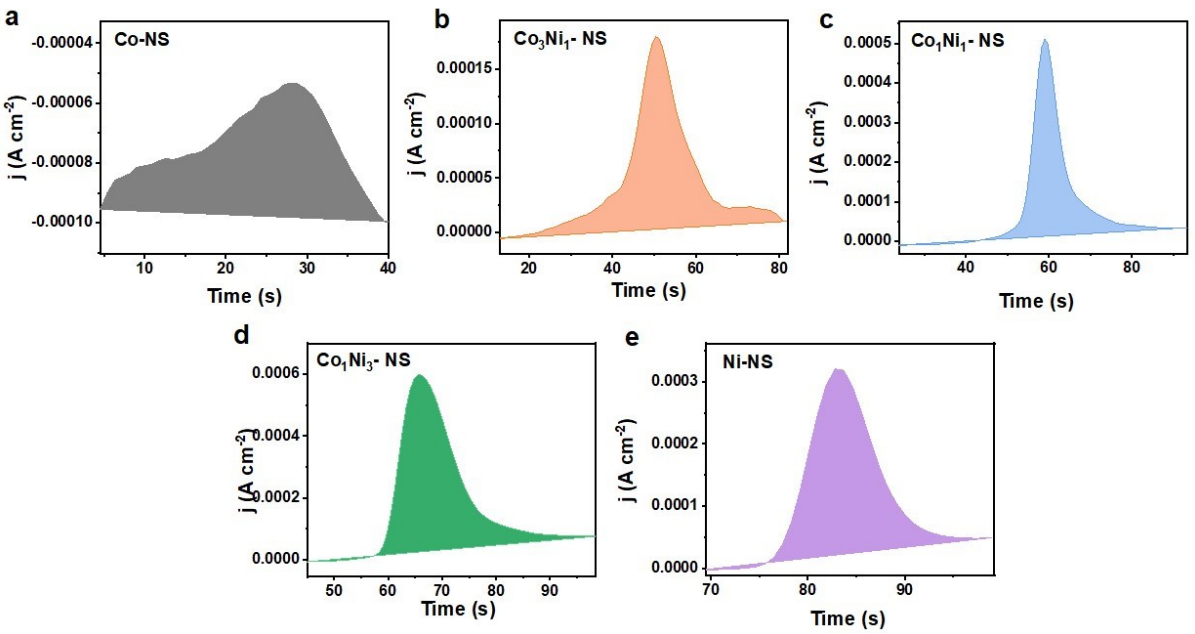

Fig. S15: Determination of integrated charge associated with oxidation of $Co_xNi_{1-x}(OH)_2$. The shaded region represents the integrated area i. e., the quantity of electric charge (Q) for Co-NS, Co_3Ni_1-NS, Co_1Ni_1-NS, Co_3Ni_1-NS, and Ni-NS was measured to be 0.0031, 0.0027, 0.005, 0.0084, and 0.0027, respectively.

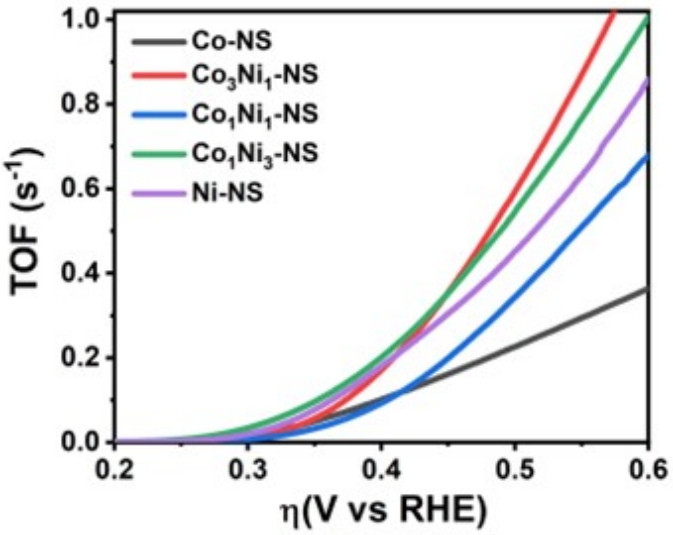

Fig. S16: TOF plot of $Co_xNi_{1-x}(OH)_2$ NS as a function of overpotential

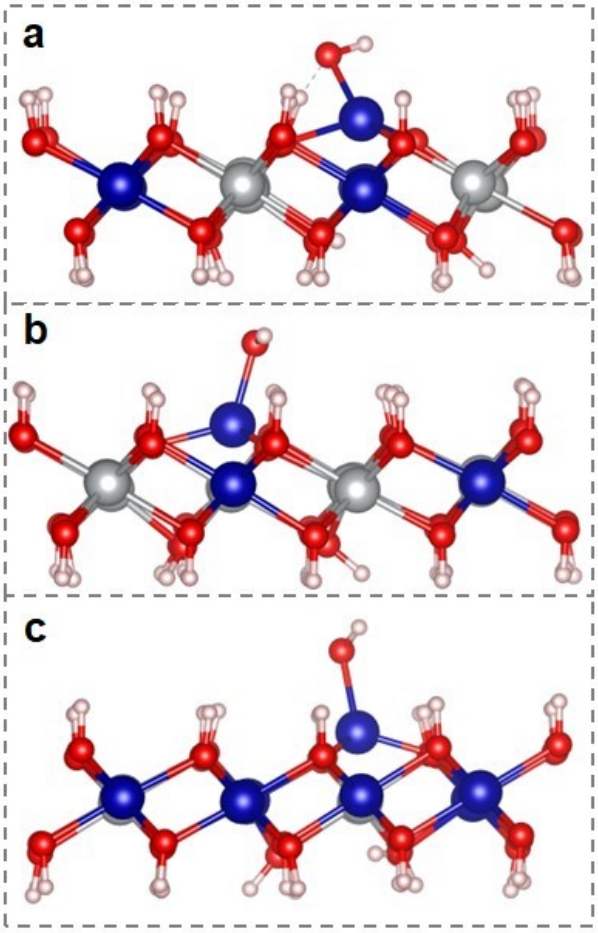

Fig. S17: Structures showing the adsorption of the OH* intermediate on CoNi hydroxide with Co and Ni ratios of (a) 1:3, (b) 1:1, and (c) 3:1, respectively.

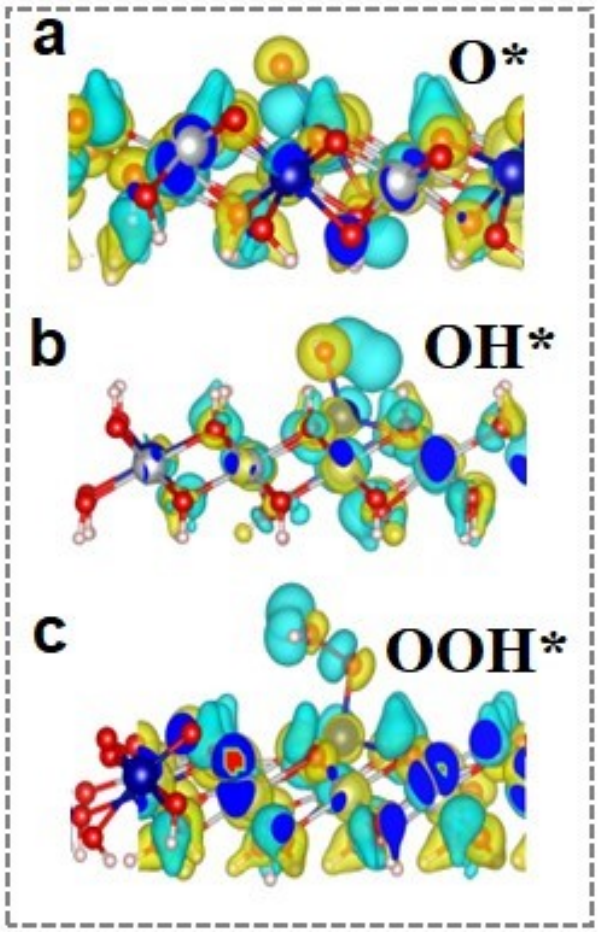

Fig. S18: Charge density difference plots of intermediates steps (a) O*, (b) OH*, and (c) OOH* respectively.

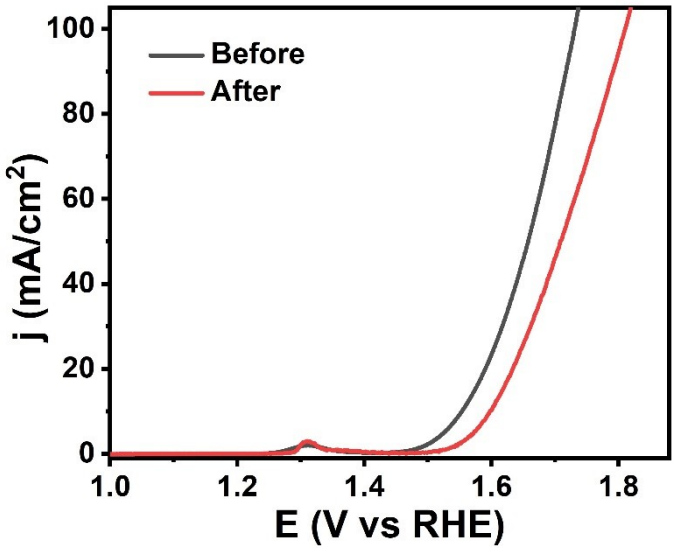

Fig. S19: The LSV curve of Co_1Ni_3-NS before and after CA measurement.

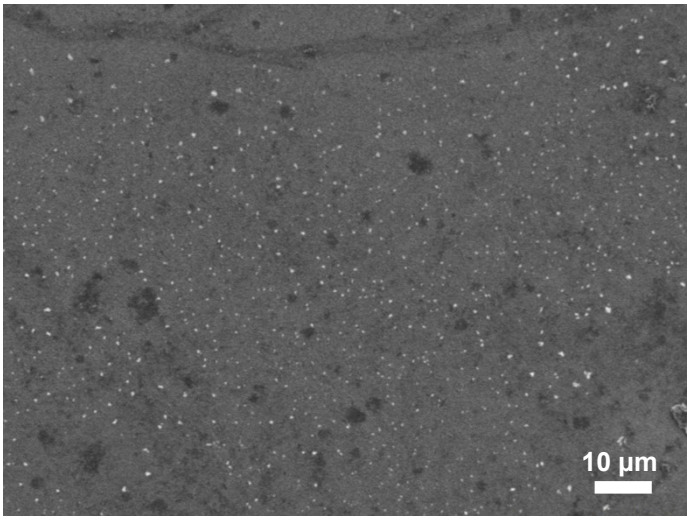

Fig. S20: low-magnification FESEM image of Co_1Ni_3-NS electrode after OER operation.

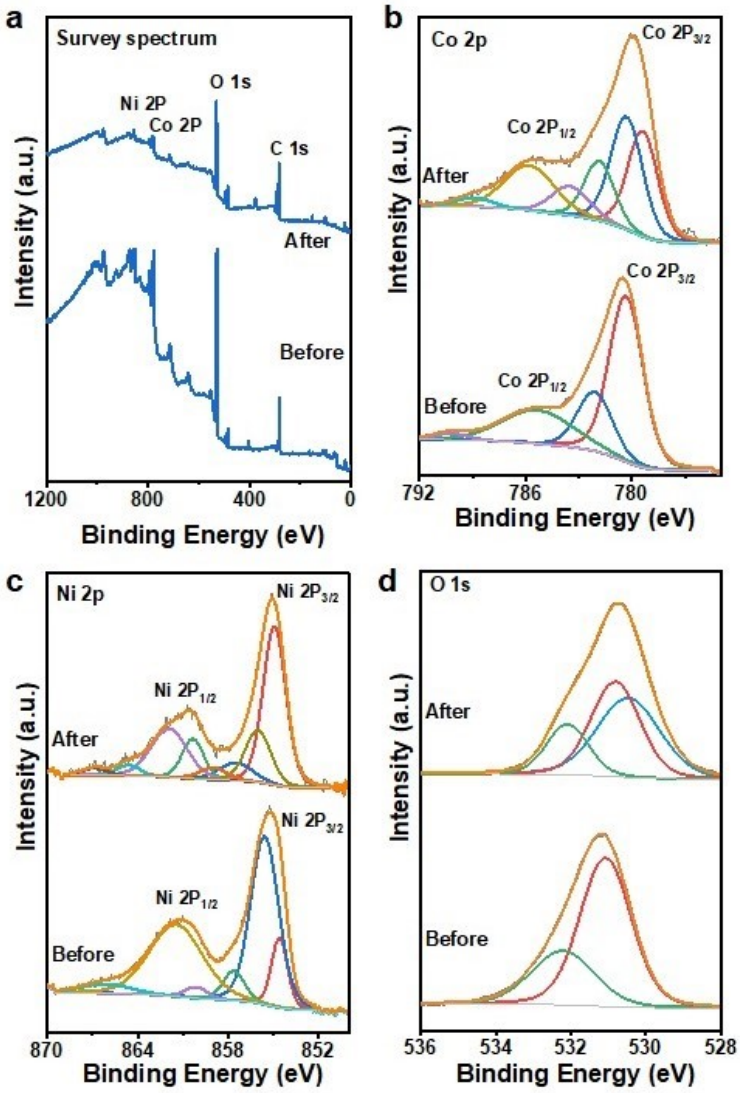

Fig. S21: XPS measurements of Co_1Ni_3-NS electrode after OER stability. (a) survey spectrum, (b) high-resolution Co 2p, (c) Ni 2p, and (d) O 1s spectrum.

Table S1: Synthesis conditions of the $Co_xNi_{1-x}(OH)_2$ NS samples with different ratios of Co/Ni.

Samples	Co: Ni Ratio	$Co(NO_3)_2.6H_2O$ (mM)	$Ni(NO_3)_2.6H_2O$ (mM)	HMTA (mM)
Co-NS	1: 0	10	0	10
Co_3Ni_1-NS	3: 1	7.5	2.5	10
Co_1Ni_1-NS	1: 1	5.0	5.0	10
Co_1Ni_3-NS	1: 3	2.5	7.5	10
Ni-NS	0: 1	0	10	10

Table S2: The DFT energies (E), entropy terms (TS), and standard zero-point energy (ZPE) values for the free molecules. From the DFT energy (E) of H_2O and H_2 we have calculated for the rest of them using the formulas E1, E2, E3, E4.

Molecules	**TS**	**ZPE**	**G**	**E(DFT)**
O_2	0.64	0.242	-9.83864	
H_2O	0.67	0.592	-14.3001	-14.2221
OH	0.41	0.271	-10.0115	
H_2	0.41	0.26	-6.92078	-6.77078
O	0.32	0.121	-4.91932	
H^+	0.205	0.13	-4.28862	

Table S3: The parameters of $Co_xNi_{1-x}(OH)_2$ NS measured from EIS fitting.

Samples	**Co-NS**	**Co_3Ni_1-NS**	**Co_1Ni_1-NS**	**Co_1Ni_3-NS**	**Ni-NS**
R_{ct} (Ω)	0.09	0.20	0.27	0.23	0.87
R_s (Ω)	0.05	0.01	0.03	0.05	0.09

Table S4: Comparative supercapacitors performance of selected materials compared with Co_1Ni_3-NS.

Sr. No.	Electrode	C_{areal} (mF cm^{-2})	C_{vol} (Fcm^{-3})	ED ($mWhcm^{-3}$)	PD (Wcm^{-3})	Stability	Ref.
1	Ni@CoNi-MOF film	1.43	100	31.3	3.8	100/ 10,000	[13]
2	Zn-Ni-Co TOH	2.14	5.4	2.43	0.006	153/ 10,000	[14]
3	NiCo-LDH nanosheets	6.37	249	7.4	0.103	90/ 1000	[15]
4	A-NiCo-LDH/NF	_	_	3.1	0.0042	92/ 70,000	[16]
5	$Co(OH)_2$/np-NiOxHy@Ni	_	1421	59.2	1.9	73/2000	[17]
6	$NiCoO_2$/Ni(OH)2/Co$(OH)_2$ nanosheets	_	_	37.4	0.155	109/ 1000	[18]
7	Ni–Co oxyhydroxides	20.9		19.5	0.204	91/7000	[19]
8	MoCoFe-based hydroxides	3354	_	1.27	3.75	91/3000	[20]
9	CoZnNioxyphosphide nanoarrays	-	2096	71.8	0.96	85/6000	[21]
10	CoZnNiS@CNTs/rGO film	-	1727	65.2	1.3	90/10,000	[22]
11	Co_1Ni_3-NS	2.95	3783	336	153	75 %/ 10,000	this work

Table S5:OER performance of various electrode materials with Co and Ni sites.

Sr. No.	Catalyst	Electrolyte	η_{10} (mV vs RHE)	Tafel slope (mV dec^{-1})	Stability	Ref.
1	NiCo@LDH-NC	1M KOH	330 at 10 mA cm^{-2}	36.4	12 h	[23]
2	NCZO/Mn–$Ni(OH)_2$/rGO/NF	1M KOH	407 at 50 mA cm^{-2}	62.6	8,000 cycles	[24]
3	NHCoMX	1M KOH	310 at 10 mA cm^{-2}	65	10 h	[25]
4	Ag@$CoNi(OH)_2$/NF	0.1 KOH	275 at 50 mA cm^{-2}	79.8	50 h	[26]
5	$Co_{50}Ni_{50}$	1M NaOH	375 at 10 mA cm^{-2}	55.6	50 h	[27]
6	$Ni_{0.3}Co_{0.74}Se$	1M KOH	397 at 10 mA cm^{-2}	76	8 h	[28]
7	Co_1Ni_3-NS	1M KOH	318 at 10 mA cm^{-2}	61	12 h	This work

Table S6: The overall electrocatalytic activity results of $Co_xNi_{1-x}(OH)_2$ NS.

Sample	Onset potential (V vs RHE)	η_{10} (mV vs RHE)	Tafel (mV dec^{-1})	R_s (Ω)	R_{ct} (Ω)	C_{dl} (μFcm^{-2})	ECSA (cm^2)
Co-NS	1.564	481	81	3.15	37.2	7.5	0.187
Co_3Ni_1-NS	1.557	401	73	3.15	5.83	11.0	0.275
Co_1Ni_1-NS	1.544	377	71	3.15	4.78	11.6	0.290
Co_1Ni_3-NS	1.478	318	61	3.15	3.73	13.0	0.325
Ni-NS	1.544	409	79	3.15	8.83	8.1	0.202

Table S7: Calculated quantitative parameters for monometallic and bimetallic $Co_xNi_{1-x}(OH)_2$ NS.

Sample	Stoichiometric coefficient of Co (x)	Stoichiometric coefficient of Ni (y)	Effective density (ρ, g cm^{-3})	Molecular weight (M, g mol^{-1})
Co-NS	1	0	3.60	92.94
Co_3Ni_1-NS	0.56	0.23	4.72	80.51
Co_1Ni_1-NS	0.23	0.26	7.42	64.59
Co_1Ni_3-NS	0.21	0.57	5.06	79.84
Ni-NS	0	1	4.10	92.70

Table S8: Bader charge values on the Oxygen atom, after adsorption and bonding with Co site for different intermediate states.

Intermediates	Valence charge of the oxygen atom	After adsorption	Charge gained
OH*	6	7.1992	1.199e
O*	6	6.7591	0.759e
OOH*	6	6.5249	0.524e

References

1. S. Ashok Patil, P. B. Jagdale, N. Barman, A. Iqbal, A. Sfeir, S. Royer, R. Thapa, A. Kumar Samal and M. Saxena, *J. Colloid Interface Sci.*, 2024, **674**, 587-602.
2. P. B. Jagdale, S. A. Patil, A. Sfeir, N. Barman, A. Iqbal, S. Royer, R. Thapa, A. K. Samal, D. Ghosh and M. Saxena, *Mater. Today Energy*, 2024, **44**, 101608.
3. P. B. Jagdale, S. A. Patil, M. Pathak, P. Bhol, A. Sfeir, S. Royer, A. K. Samal, C. S. Rout and M. Saxena, *J. Mater. Chem. A*, 2024, **12**, 17350-17359.
4. R. A. Nickell, W. H. Zhu, R. U. Payne, D. R. Cahela and B. J. Tatarchuk, *J. Power Sources*, 2006, **161**, 1217-1224.
5. Y. Zhao, Y. Wang, Y. Dong, C. Carlos, J. Li, Z. Zhang, T. Li, Y. Shao, S. Yan, L. Gu, J. Wang and X. Wang, *ACS Energy Lett.*, 2021, **6**, 3367-3375.
6. P. Tian, Y. Yu, X. Yin and X. Wang, *Nanoscale*, 2018, **10**, 5054-5059.
7. G. Kresse and J. Hafner, *Phys. Rev. B.*, 1993, **47**, 558-561.
8. X. Tan, S. Jia, X. Song, X. Ma, J. Feng, L. Zhang, L. Wu, J. Du, A. Chen, Q. Zhu, X. Sun and B. Han, *Chem. Sci.*, 2023, **14**, 8214-8221.
9. G. Kresse and D. Joubert, *Phys. Rev. B.*, 1999, **59**, 1758-1775.
10. P. E. Blöchl, *Phys. Rev. B.*, 1994, **50**, 17953-17979.
11. J. P. Perdew, K. Burke and M. Ernzerhof, *Phys. Rev. Lett.*, 1996, **77**, 3865-3868.
12. S. Grimme, J. Antony, S. Ehrlich and H. Krieg, *J. Chem. Phys.*, 2010, **132**, 154104.
13. M. Hong, C. Zhou, S. Xu, X. Ye, Z. Yang, L. Zhang, Z. Zhou, N. Hu and Y. Zhang, *J. Power Sources*, 2019, **423**, 80-89.

14. Z.-H. Huang, F.-F. Sun, M. Batmunkh, W.-H. Li, H. Li, Y. Sun, Q. Zhao, X. Liu and T.-Y. Ma, *J. Mater. Chem. A*, 2019, **7**, 11826-11835.
15. L. Zhi, W. Zhang, L. Dang, J. Sun, F. Shi, H. Xu, Z. Liu and Z. Lei, *J. Power Sources*, 2018, **387**, 108-116.
16. D. Zha, Y. Fu, L. Zhang, J. Zhu and X. Wang, *J. Power Sources*, 2018, **378**, 31-39.
17. F. Zhao, D. Zheng, Y. Liu, F. Pan, Q. Deng, C. Qin, Y. Li and Z. Wang, *Chem. Eng. J.*, 2021, **415**, 128871.
18. T. Qin, H. Li, R. Ren, J. Hao, Y. Wen, Z. Wang, J. Huang, D. He, G. Cao and S. Peng, *CrystEngComm*, 2018, **20**, 6519-6528.
19. X. Ren, M. Li, L. Qiu, X. Guo, F. Tian, G. Han, W. Yang and Y. Yu, *J. Mater. Chem. A*, 2023, **11**, 5754-5765.
20. Q. T. Nguyen, U. T. Nakate, J. Chen, D. T. Tran and S. Park, *Compos. B Eng.*, 2023, **252**, 110528.
21. X. Chen, Y. Liu, Q. Yang, L. Li, Y. Ying and W. Shi, *J. Colloid Interface Sci.*, 2022, **610**, 427-437.
22. Y. Liu, N. Xin, Q. Yang and W. Shi, *J. Colloid Interface Sci.*, 2021, **583**, 288-298.
23. R. Patil, A. Rajput, N. Kumar, O. Agrawal, M. Ujihara, R. R. Salunkhe, B. Chakraborty and S. Dutta, *ACS Appl. Eng. Mater.*, 2023, **1**, 2018-2028.
24. S. Zhou, H. Zhao, E. Fan, Z. Zhang, G. Dong, W. Zhang, Y. Zang, M. Zhao, D.-F. Chai and X. Huang, *Ceram. Int.*, 2024.
25. A. R. Manchuri, K. C. Devarayapalli, B. Kim, Y. Lim and D. S. Lee, *GREEN ENERGY ENVIRON.*, 2024.
26. Y. Li, J. Han, W. Bao, J. Zhang, T. Ai, M. Yang, C. Yang and P. Zhang, *J. Energy Chem.*, 2024, **90**, 590-599.
27. F. Florian Le, Y. Lucas, M. Elizaveta Potapova, C. Xavier Pereira Da, B. Florent, G. Nestor, S. Mariana, Z. Andreas and S. Kevin, *Journal*, 2020, **10**, 12139-12147.
28. M. Wang, Z. Dang, M. Prato, D. V. Shinde, L. De Trizio and L. Manna, *ACS Appl. Nano Mater.*, 2018, **1**, 5753-5762.